ISSN 1063-7761, Journal of Experimental and Theoretical Physics, 2012, Vol. 115, No. 1, pp. 56–67. © Pleiades Publishing, Inc., 2012.
Original Russian Text © A.A. Skorynin, V.A. Bushuev, B.I. Mantsyzov, 2012, published in Zhurnal Eksperimental'noi i Teoreticheskoi Fiziki, 2012, Vol. 142, No. 1, pp. 64–76.

ATOMS, MOLECULES, OPTICS

Dynamical Bragg Diffraction of Optical Pulses in Photonic Crystals in the Laue Geometry: Diffraction-Induced Splitting, Selective Compression, and Focusing of Pulses

A. A. Skorynin*, V. A. Bushuev, and B. I. Mantsyzov**

Moscow State University, Moscow, 119991 Russia

**e-mail: skoraleks@ya.ru*

***e-mail: mantsyzov@phys.msu.ru, bmantsyzov@gmail.com*

Received December 17, 2011

Abstract—A theory for the dynamical Bragg diffraction of a spatially confined laser pulse in a linear photonic crystal with a significant modulation of the refractive index in the Laue geometry has been developed. The diffraction-induced splitting of a spatially confined pulse into the Borrmann and anti-Borrmann pulses localized in different regions of the photonic crystal and characterized by different dispersion laws is predicted. The selective compression or focusing of one of these pulses with the simultaneous broadening or defocusing of the other pulse is shown to be possible.

DOI: 10.1134/S1063776112060167

1. INTRODUCTION

The diffraction phenomena that emerge when electromagnetic radiation in various wavelength ranges interacts with periodic structures have a number of common patterns. For example, there exist the regions of selective Bragg reflection or the so-called photonic forbidden bands in the case of X-ray [1], optical or radio wave [2] diffraction in the Bragg geometry and the Borrmann [3, 4] and pendulum [1, 5, 6] effects in the case of dynamical Bragg diffraction in the Laue scheme. The dynamical diffraction in the Lauer geometry "for transmission", when the transmitted and diffracted waves propagate into the structure, was investigated previously for a weak modulation $\delta_0 = n_1 - n_2$ of the refractive index of the medium [7–12] mainly in the problems of X-ray propagation in crystals ($\delta_0 \sim 10^{-5}$) [1]. The anomalously weak absorption of X-rays in crystals or the Borrmann effect [3], which results from the localization of different field modes in different regions of the crystal, has long been explained. The weakly absorbed field, i.e., the Borrmann mode, is localized predominantly between the crystal planes in the region of a low electron density, while the strongly absorbed anti-Borrmann mode is localized mainly on the crystal planes. If we choose a sufficiently thin crystal in which the anti-Borrmann mode has no time to be absorbed and, consequently, all radiation eigenmodes in the crystal exist at each point of the medium, then the pendulum effect or the pendulum solution is observed [1]. In this case, as the radiation propagates in the crystal, the energy of the transmitted wave is transferred periodically completely into the diffracted wave and back [1, 5, 6].

The main significant differences in the X-ray and optical diffraction effects arise when the large modulation depth of the refractive index for the structure ($\delta_0 \sim 0.1$) and the nonlinearity of the laser radiation–photonic crystal (PC) interaction are taken into account [13, 14]. Apart from purely nonlinear effects—an increase in the generation efficiency of nonlinear signals due to the field localization in the medium at the edge of the photonic forbidden band [15] and quasi-phase matching both in the Bragg geometry [16] and in the Laue scheme in crystals with random [17] and regular [18] domain structures as well as the propagation of Bragg solitons [13, 14]—new dynamical linear and nonlinear phenomena typical of media with a large contrast of the refractive index appear in PCs. Previously, the diffraction-induced splitting of laser pulses in linear [6] and nonlinear resonant [4] PCs was predicted for the dynamical diffraction of radiation in the Laue scheme. In the case of linear PCs, the pulses were assumed to be in the form of plane quasi-monochromatic wave packets with an unbounded wave front in the cross section. Pulse splitting results from the localization of the Borrmann and anti-Borrmann modes in different spatial PC regions. This leads to different dispersion laws for the two modes and to the propagation of two pulses, the Borrmann and anti-Borrmann ones, with different group velocities in the PC.

A similar effect was also predicted for the case of discrete diffraction in a lattice of coupled waveguides, where the initial pulse is split into eigenmode pulses with different group velocities [19, 20]. The compression and change of the pulse profile upon diffraction in

the Laue scheme was previously considered in optics for media with a low contrast of the refractive index [9, 10] in the case of relatively optically thin structures, where the Borrmann and anti-Borrmann modes do not separate spatially and there is no diffraction-induced pulse splitting, but only the regime of the pendulum solution is realized.

In this paper, we analytically solve the boundary-value problem of Bragg diffraction in the Laue geometry for a spatially confined short laser pulse in a one-dimensional linear PC (Fig. 1) with a relatively large modulation of the refractive index typical of PCs composed of semiconductor and dielectric materials, for example, porous silicon or oxidized porous silicon [21]. The incident pulse is represented as a two-dimensional Fourier decomposition into plane monochromatic waves with different frequencies and wave vectors. Subsequently, once the Fourier amplitudes of each of the plane waves inside the PC have been determined in the two-wave approximation, we perform a Fourier synthesis and find the field strengths of the forward (transmitted) and diffracted pulses at different PC points at a specific instant of time. We show that the diffraction-induced pulse splitting (DIPS) in a one-dimensional PC takes place for spatially confined laser pulses with transverse sizes greater than or of the order of 20 μm. The dynamics and parameters of the separated pulses can be efficiently controlled due to different lattice-induced dispersions for the Borrmann and anti-Borrmann pulse fields and due to different spatial localizations of these pulses in the PC after the diffraction-induced splitting of the input signal. We predict the selective compression of a frequency-modulated pulse, i.e., the compression of either the fast Borrmann or slow anti-Borrmann pulses, depending on the sign of the input signal frequency modulation. The selective pulse focusing is also shown to be possible.

2. THE DIFFRACTION-INDUCED SPLITTING OF A SPATIALLY CONFINED OPTICAL PULSE

Consider a one-dimensional photonic crystal that consists of optically isotropic, periodically alternating layers with thicknesses d_1, d_2 and refractive indices n_1, n_2. The layers are perpendicular to the PC surface (Fig. 1). An arbitrary light pulse with the following electric field is incident on the PC at an angle θ to the normal to its surface:

$$E_{\text{in}}(\mathbf{r}, t) = A_{\text{in}}(\mathbf{r}, t)\exp(i\mathbf{k}_0 \cdot \mathbf{r} - i\omega_0 t), \qquad (1)$$

where A_{in} is generally a slowly changing complex amplitude, ω_0 is the central frequency of the signal, $k_0 = |\mathbf{k}_0| = \omega_0/c = 2\pi/\lambda_0$, λ_0 is the central wavelength, c is the speed of light in a vacuum, $k_{0x} = k_0\sin\theta$, $k_{0z} = k_0\cos\theta$, the x axis is directed along the PC surface, and the z axis is directed into the crystal along the normal to its surface. For simplicity, we consider a pulse with an s field polarization.

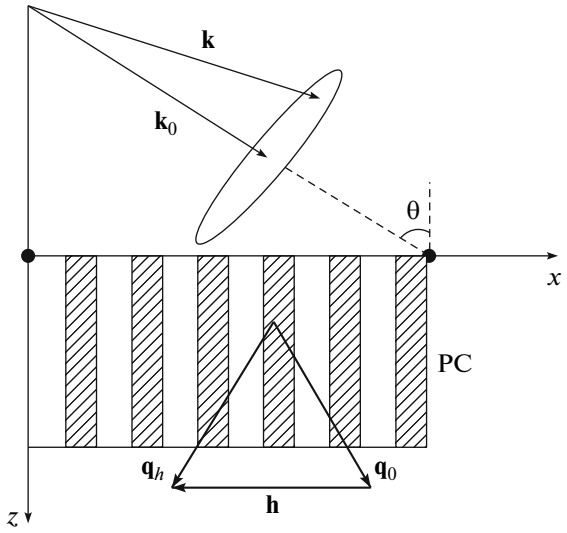

Fig. 1. Pulse diffraction scheme in the Laue geometry in a one-dimensional photonic crystal.

The complex field $E(\mathbf{r}, t)$ in the PC obeys the wave equation

$$\Delta E(\mathbf{r}, t) - \frac{\varepsilon(x)}{c^2}\frac{\partial^2 E(\mathbf{r}, t)}{\partial t^2} = 0, \qquad (2)$$

where $\varepsilon(x) = n^2(x)$ is the complex permittivity and $\Delta = \partial^2/\partial x^2 + \partial^2/\partial z^2$ is the Laplace operator. We will represent the refractive index of the medium $n(x)$ in the PC as a function of the x coordinate as

$$n(x) = n_e + \Delta n(x),$$

where

$$n_e = (n_1 d_1 + n_2 d_2)/d = n_2 + \delta_0\xi$$

is the average refractive index, $\delta_0 = n_1 - n_2$ is the modulation of the refractive index, $\xi = d_1/d$, and $d = d_1 + d_2$ is the period of the structure. The function $\Delta n(x) = \delta_0(1 - \xi)$ in the layers with thicknesses d_1 and $\Delta n(x) = -\delta_0\xi$ in the layers with thicknesses d_2.

Let us represent the field (1) of the incident pulse on the PC surface $z = 0$ as a two-dimensional Fourier decomposition, i.e., as a set of plane monochromatic waves with amplitudes $E_{\text{in}}(k_x, \omega)$, frequencies $\omega = \omega_0 + \Omega$, and wave vectors $\mathbf{k}$, where $|\mathbf{k}| \equiv k = \omega/c$, whose projections are defined by the relations $k_x = k_{0x} + K$ and $k_z = \sqrt{(\omega/c)^2 - k_x^2}$:

$$E_{\text{in}}(x, t) = \int_{-\infty}^{\infty}\int_{-\infty}^{\infty} E_{\text{in}}(k_x, \omega)\exp(ik_x x - i\omega t)dk_x d\omega,$$

where the spectral angular amplitudes

$$E_{\text{in}}(k_x, \omega) \equiv A_{\text{in}}(K, \Omega) = \frac{1}{4\pi^2}\int_{-\infty}^{\infty}\int_{-\infty}^{\infty} A_{\text{in}}(x, t)\exp(-iKx + i\Omega t)dxdt. \quad (3)$$

Consider a PC with a significant modulation of the refractive index ($\delta_0 \le 0.3$), which allows us to consider the pulse diffraction in the two-wave approximation, when two "strong" waves exists near the Bragg condition $h = 2k_0\sin\theta_B$ in the PC—the transmitted, E_0, and diffracted, E_h, ones with wave vectors $\mathbf{q}_0$ and $\mathbf{q}_h = \mathbf{q}_0 + \mathbf{h}$ for each spectral angular field component, where $\mathbf{h}$ is the reciprocal lattice vector, $|\mathbf{h}| \equiv h = 2\pi/d$, and θ_B is the Bragg angle for radiation with a central frequency ω_0. A more accurate criterion of applicability for the two-wave approximation will be formulated below. In this case, in the range $0 \le z \le L$, where L is the PC thickness, the total field

$$E(\mathbf{r}, t) = E_0(\mathbf{r}, t) + E_h(\mathbf{r}, t) \quad (4)$$

is a coherent superposition of the incident, E_0, and diffracted, E_h, pulse fields. Since the tangential components of the wave vectors $q_{0x}(K) = k_x = k_{0x} + K$ are continuous on the $z = 0$ surface, we seek the field in the PC in the form

$$E_g(x, z, t) = \int_{-\infty}^{\infty}\int_{-\infty}^{\infty} A_g(K, \Omega) \times \exp[i(q_{0x} - g)x + iq_{0z}z - i\omega t]dKd\Omega, \quad (5)$$

where $g = 0, h$; h is the magnitude of the reciprocal lattice vector whose projections are $h_x = -h$ and $h_z = 0$; $q_{0z} = q_{hz}$ are the z projections of the wave vectors in the PC (see Eq. (12) below), which can be determined from the wave equation (2).

The permittivity $\varepsilon(x)$ in the two-wave approximation is [6]

$$\varepsilon(x) = \chi_0 + \chi_h e^{-ihx} + \chi_{-h}e^{ihx}, \quad (6)$$

where χ_0, χ_h, and χ_{-h} are the Fourier components of the permittivity defined by the relations

$$\chi_0 = n_e^2 + \delta_0^2(\xi - \xi^2),$$

$$\chi_h = \frac{i}{\pi}\left(n_e\delta_0 + \delta_0^2\frac{1-2\xi}{2}\right)(1 - e^{2i\pi\xi}),$$

$$\chi_{-h} = -\frac{i}{\pi}\left(n_e\delta_0 + \delta_0^2\frac{1-2\xi}{2}\right)(1 - e^{-2i\pi\xi}).$$

Substituting Eqs. (4), (5), and (6) into the wave equation (2) leads to the following system of dynamical equations for the field amplitudes A_0 and A_h in (5):

$$(k^2\chi_0 - q_{0x}^2 - q_{0z}^2)A_0 + k^2\chi_{-h}A_h = 0,$$
$$[k^2\chi_0 - (q_{0x} - h)^2 - q_{0z}^2]A_h + k^2\chi_h A_0 = 0. \quad (7)$$

Let us introduce convenient designations:

$$\gamma_0 = \frac{1}{k}\sqrt{k^2\chi_0 - q_{0x}^2}, \quad \alpha = \frac{h}{k^2}(2q_{0x} - h), \quad (8)$$

$$\beta = \frac{q_{0z}^2 - k^2\gamma_0^2}{k^2}, \quad (9)$$

where the function $\alpha(K, \Omega)$ defines the degree of detuning from the exact Bragg condition $\alpha = 0$. System (7) will then be written in compact form:

$$\beta A_0 - \chi_{-h}A_h = 0, \quad (10a)$$

$$(\beta - \alpha)A_h - \chi_h A_0 = 0. \quad (10b)$$

A quadratic equation for the variable β (9) is derived from the condition for the solution of system (10) for the amplitudes A_0 and A_h being nontrivial. Its solution has two roots:

$$\beta_{1,2} = \frac{1}{2}\left(\alpha \mp \sqrt{\alpha^2 + 4\chi_h\chi_{-h}}\right). \quad (11)$$

We will assume that only the waves propagating into the structure exist in a semi-infinite PC. Therefore, given (9), we will obtain the following final expression for the sought-for z projections of the wave vectors in the PC:

$$q_{0z}^{(1,2)} = k\sqrt{\gamma_0^2 + \beta_{1,2}}. \quad (12)$$

In addition, a simple relation between the field amplitudes A_h and A_0 follows from Eq. (10a):

$$A_{hj} = R_j A_{0j}, \quad j = 1, 2, \quad R_{1,2} = \beta_{1,2}/\chi_{-h}.$$

It should be emphasized that, in contrast to [6], solution (12) and quantities (8) and (9) are exact without any expansion in terms of the parameters K/k_0, Ω/ω_0, and $(\theta - \theta_B)/\theta_B$.

The Fourier amplitudes of the fields $A_{0,h}(K, \Omega)$ can be determined from the conditions for the electric and magnetic fields being continuous on the PC entrance surface $z = 0$:

$$A_{\text{in}} + A_s = A_{01} + A_{02},$$
$$k_z(A_{\text{in}} - A_s) = q_{0z}^{(1)}A_{01} + q_{0z}^{(2)}A_{02}, \quad (13)$$
$$R_1A_{01} + R_2A_{02} = 0,$$

where A_s is the amplitude of the specularly reflected wave. Taking into account the reflection of the transmitted and diffracted pulses from the lower PC surface does not change the main features of DIPS. The solution of system (13) is

$$A_{01} = -[(1 + R_s)R_2/R_{12}]A_{\text{in}},$$
$$A_{02} = [(1 + R_s)R_1/R_{12}]A_{\text{in}}, \quad (14)$$

where $R_{12} = R_1 - R_2$, $R_s = A_s/A_{\text{in}} = (k_z - f_s)/(k_z + f_s)$ is the diffraction-modified Fresnel reflection coefficient, and $f_s = (q_{0z}^{(2)}R_1 - q_{0z}^{(1)}R_2)/R_{12}$.

As a result, we obtain the following expression for the total field (4) in the PC:

$$E(x, z, t) = [A_0(x, z, t) + A_h(x, z, t)\exp(-ihx)] \times \exp(ik_{0x}x - i\omega_0 t), \quad (15)$$

where

$$A_g(x, z, t) = \int_{-\infty}^{\infty}\int_{-\infty}^{\infty} B_g A_{\text{in}}(K, \Omega) \times \exp(iKx - i\Omega t)dKd\Omega, \quad (16)$$

$$B_g = A_{\text{in}}^{-1}\sum_{j=1,2} A_{gj}\exp(iq_{0z}^{(j)}z), \quad g = 0, h,$$

$B_0 = T(z)$ and $B_h = R(z)$ are, respectively, the amplitude transmission and reflection coefficients of plane waves in a PC layer of thickness z. The total field (15) can also be represented as the sum of the fields of both modes:

$$E(x, z, t) = [A_1(x, z, t) + A_2(x, z, t)] \times \exp(ik_{0x}x - i\omega_0 t),$$

$$A_j(x, z, t) = \int_{-\infty}^{\infty}\int_{-\infty}^{\infty} B_j A_{\text{in}}(K, \Omega) \times \exp(iKx - i\Omega t)dKd\Omega, \quad (17)$$

$$B_j = A_{\text{in}}^{-1}\exp(iq_{0z}^{(j)}z)\sum_{g=0,h} A_{gj}\exp(-igx), \quad j = 1, 2.$$

Thus, four waves exist for each plane-wave field component: two with wave vectors $\mathbf{q}_0^{(1)}$ and $\mathbf{q}_h^{(1)}$ for the transmitted and diffracted waves, the Borrmann mode, and two with wave vectors $\mathbf{q}_0^{(2)}$ and $\mathbf{q}_h^{(2)}$, the anti-Borrmann mode (12). The transmitted and diffracted waves of each mode have pairwise identical projections of the wave vectors onto the z axis and pairwise identical group velocities in the x and z directions (see Eqs. (23) and (24) below). In addition, the projections of the wave vectors onto the x axis for the transmitted and diffracted waves differ by the reciprocal lattice vector, a constant. Therefore, if the Bragg condition is fulfilled exactly, then the sums of these waves with identical indices are two standing waves in the x direction. These modes have different phase and group velocities in the x and z directions because of the difference between the effective refractive indices

$$n_{ej}(K, \Omega) = |\mathbf{q}^{(j)}|/k = \sqrt{\chi_0 + \beta_j}$$

(see Eqs. (8), (11), and (12)) due to the lattice-induced dispersion, which, as a rule, exceeds considerably the material dispersion of the PC layers.

Depending on the index j, the field of each mode is predominantly localized in PC layers with smaller (the Borrmann mode, $j = 1$) or larger (the anti-Borrmann mode, $j = 2$) refractive indices n_j and the corresponding absorption coefficient $\mu_j = 2k_0 \text{Im}\, n_j$. Figure 2 presents the dispersion curves $q_{0z}^{(1,2)}(q_{0x})$ (12) for the Borrmann and anti-Borrmann modes, which are isofrequency sections of the PC dispersion surface $\omega(\mathbf{q})$. Therefore, the angle of incidence shown on the upper axis can be uniquely associated with each projection of the wave vector. To demonstrate the influence of the lattice-induced dispersion, the same figure presents the dependence for a homogeneous material with the average PC refractive index $\sqrt{\chi_0}$ for which the z projection of the wave vector is equal to $k\gamma_0$. The arrows indicate the directions of the normal to the dispersion curves corresponding to the energy propagation directions for the Borrmann and anti-Borrmann modes [1].

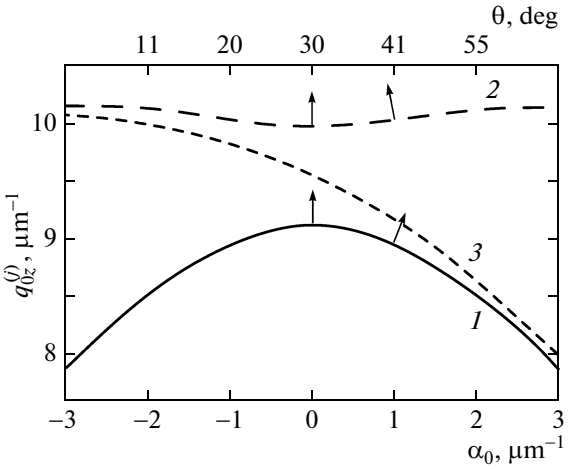

Fig. 2. Dispersion curves for the Borrmann (curve *1*) and anti-Borrmann (curve *2*) modes as well as for a homogeneous medium with the average PC refractive index $\sqrt{\chi_0}$ (*3*) as a function of the variable $\alpha_0 = q_{0x} - h/2$ at a constant frequency. The PC and radiation parameters are $n_1 = 1.7$ and $\delta_0 = 0.2$; the period is $d = 1$ μm, $\xi = 0.5$, and the wavelength is $\lambda_0 = 1$ μm. The arrows indicate the directions of the group velocities for the Borrmann and anti-Borrmann modes (the normals to the curves) at angular deviations of 0° and 11° from the exact Bragg condition.

Figure 3 shows the intensities of both modes $I_j(x) = |A_j(x)|^2$ $(j = 1, 2)$ in various PC z sections measured in units of the extinction depth $\Lambda = \lambda_0\gamma_{0r}/2|\chi_h|$, where $\gamma_{0r} = \text{Re}\sqrt{\chi_0 - (q_{0x}/k)^2}$. The quantity 2Λ is equal to the period of the pendulum solution, i.e., the effect of complete energy transfer from the transmitted wave E_0 into the diffracted one E_h and back. We see from our comparison of Figs. 3a and 3b that the anti-Borrmann mode (curve *2*) is suppressed with increasing z as a result of its localization in layers with a larger absorption coefficient.

Let us now turn to discussing the optimal conditions for DIPS or the diffraction-induced splitting of

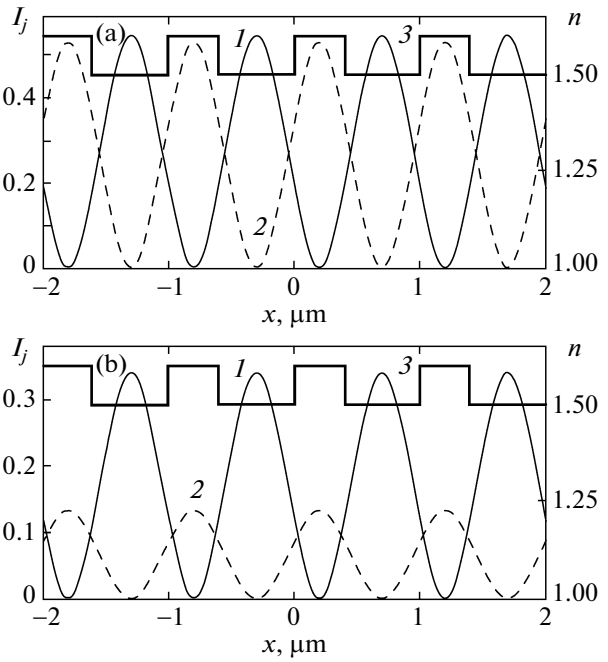

Fig. 3. Borrmann (curves *1*) and anti-Borrmann (curves *2*) modes at depths $z = 10\Lambda$ (a) and $z = 300\Lambda$ (b) as well as the profile of the real part of the refractive index (curves *3*). The PC parameters are $d = 1$ μm, $\xi = 0.4$, $n_1 = 1.6 + i \times 5 \times 10^{-5}$, $n_2 = 1.5$, the extinction depth is $\Lambda = 7.81$ μm, $\lambda_0 = 1$ μm, $\theta = \theta_B = 30°$.

an incident spatially confined pulse. It follows from Eqs. (11) and (14)–(16) that the region of efficient Bragg diffraction for a pulse in a PC is defined by the relation

$$|\alpha(K, \Omega)| \le \alpha_B = 2|\chi_h|.$$

The latter imposes a constraint on the frequency ($\Delta\Omega_0$) and angular (ΔK_0) widths of the spectrum $A_{in}(K, \Omega)$ for the incident pulse and on the detuning of the angle of incidence θ from the Bragg angle θ_B.

For a narrow spatial frequency spectrum of the incident pulse, $\Delta\Omega_0 \ll \omega_0$, $\Delta K_0 \ll k_{0x}$ near the Bragg condition $\Delta\theta \ll \theta_B$, where $\Delta\theta = \theta - \theta_B$, the detuning (8) can be expanded in terms of small parameters:

$$\alpha = 2\left(\Delta\theta + \frac{K}{k_0 \cos\theta_B}\right)\sin 2\theta_B.$$

In the case of a long-duration pulse or, for example, a beam, i.e., a wave packet with a narrow frequency spectrum ($\Delta\Omega_0 \ll \omega_0$), the angular width of the Bragg reflection peak is then

$$\Delta K_B = \frac{k_0|\chi_h|}{2\sin\theta_B}.$$

If the incident pulse is short in duration but wide enough for the width of the spatial spectrum to be neglected ($\Delta K_0/k_0 \ll \Delta\Omega_0/\omega_0$), only the waves with $K = (\Omega/c)\sin\theta$ will be present in its spectrum (3). Therefore, the frequency width of the Bragg reflection peak is defined by the expression

$$\Delta\Omega_B = \frac{\omega_0|\chi_h|}{2\sin^2\theta_B}.$$

Let a pulse with a Gaussian amplitude distribution

$$A_{in}(x, 0, t) = A\exp\left[-\left(\frac{x\cos\theta}{r_0}\right)^2 - \frac{1}{\tau^2}\left(t - \frac{x\sin\theta}{c}\right)^2\right], \quad (18)$$

where r_0 is the transverse pulse size and τ is the pulse duration, be incident on a PC. Its spectral and angular widths are $\Delta\Omega_0 \approx 2/\tau$ and $\Delta K_0 \approx 2\cos\theta/r_0$, respectively. Hence it follows that the condition $|\alpha| \le \alpha_B$ is met for a pulse with a duration $\tau > 4\sin^2\theta_B/\omega_0|\chi_h|$ and a width $r_0 > \lambda_0 \sin 2\theta_B/\pi|\chi_h|$. If, for example, $\lambda_0 \approx 1$ μm, $|\chi_h| \approx 0.2$, and $\theta_B \approx 30°$, then $\tau > 3$ fs and $r_0 > 2$ μm. In a PC with a larger contrast of the refractive index, the widths of the Bragg zones are so large that the first zone can partially overlap with higher-order zones.

To test the assumption made here about the applicability of the two-wave approximation, let us compare the spectral sizes of the Bragg zone (ΔK_B) with half the distance between the neighboring zones ($h/2$). At $\lambda_0 \approx 1$ μm, $|\chi_h| \approx 0.2$, and $\theta_B \approx 30°$, we will obtain $2\Delta K_B/h = |\chi_h|/2\sin^2\theta_B \approx 0.4$. Thus, the two-wave approximation is valid for the chosen parameters.

As a result of the difference between the z projections of the group velocities $v_z^{(j)}$ (see Eq. (23) below) for the Borrmann and anti-Borrmann modes, the Borrmann and anti-Borrmann pulses will pass through some section of the crystal at a depth $z = z_0$ with an appreciable time delay between them of the order of $2\tau = |t_1 - t_2|$, where $t_j = z_0/v_z^{(j)}$. Hence, taking into account the expansions of $q_{0z}^{(j)}$ (12) and $v_z^{(j)}$ (23) in terms of the small parameter $|\chi_h|/\chi_0$, it is easy to find that when the Bragg condition $\alpha = 0$ is met, the quantity

$$z_0 \approx \frac{2\tau c\gamma_0^3}{|\chi_h|(\chi_0 - 2\sin^2\theta_B)}.$$

This distance decreases with decreasing pulse duration and with increasing modulation depth of the refractive index. If, for example, $\lambda_0 = 1$ μm, $n_1 = 1.7$, $\delta_0 = 0.2$, $\xi = 0.5$, and $\theta_B = 30°$, then $|\chi_h| \approx 0.2$ and the splitting of an incident pulse with $\tau = 0.1$ ps into two pulses in the PC will occur at a comparatively small depth $z_0 \approx 0.5$ mm.

Consider the propagation dynamics of a spatially confined pulse in a PC. Let us introduce the total intensity of the field (15)

$$I(x, z, t) = |E(x, z, t)|^2 \quad (19)$$

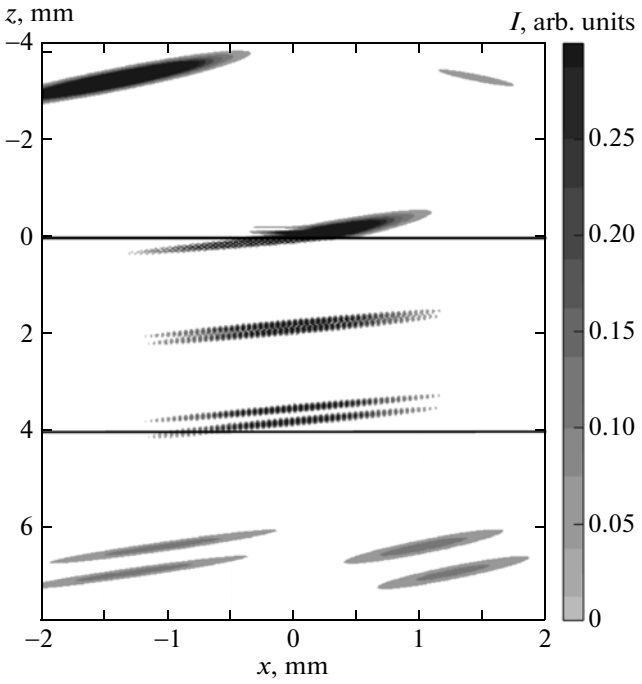

Fig. 4. Total field intensity $I(x, z)$ (19) upon DIPS of a confined pulse in a PC located between $z = 0$ mm (the upper PC boundary) and $z = 4$ mm (the lower PC boundary). The pulses are given at different instants of time. A more detailed pulse intensity distribution in the PC is presented in Fig. 5. The PC and pulse parameters are $n_1 = 1.7$, $\delta_0 = 0.2$, $d = 1$ μm, $\xi = 0.5$ and $\lambda_0 = 0.8$ μm, $\tau = 0.5$ ps, $r_0 = 0.5$ mm, $\theta = \theta_B = 23.6°$, respectively.

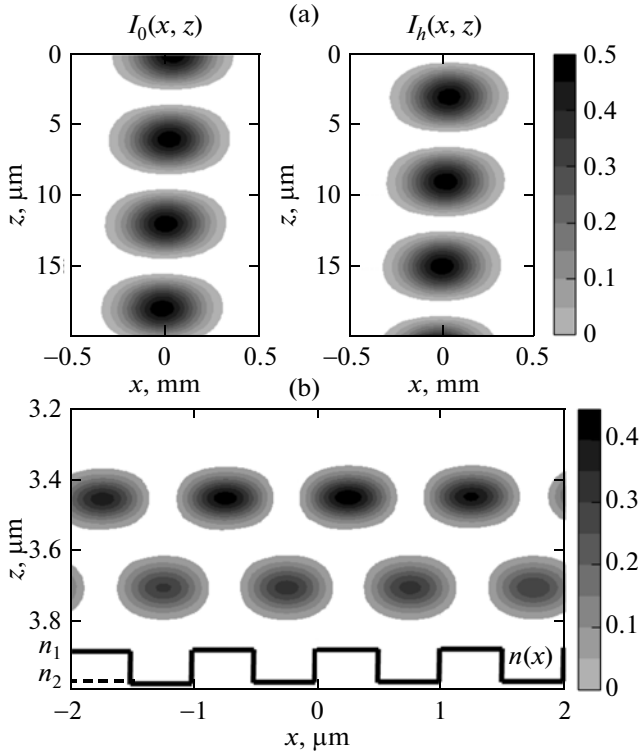

Fig. 5. Spatial field intensity distribution in a PC: (a) the field intensities of the transmitted, $I_0(x, z)$ rel. units, and diffracted, $I_h(x, z)$ rel. units, waves (20) under the pendulum effect; (b) the distribution of the total field intensity $I(x, z)$ (19) for the pulses upon DIPS; $n(x)$ is the profile of the refractive index in the PC.

and the intensities of the transmitted ($g = 0$) and diffracted ($g = h$) pulses whose amplitudes are defined by Eqs. (16),

$$I_g(x, z, t) = |A_g(x, z, t)|^2. \quad (20)$$

As we see from (15), in contrast to the total field intensity (19), the sum of the intensities for the transmitted and diffracted pulses, $I_0(x, z, t) + I_h(x, z, t)$, does not describe the small-scale intensity oscillations in the standing wave that emerges when the transmitted and diffracted waves interfere.

Figure 4 presents the spatial distribution of the total pulse field intensity $I(x, z, t = \text{const})$ (19) at various instants of time. It allows the pulse transformation dynamics at various diffraction stages to be observed on the same graph. We see that the incident pulses is refracted and partially reflected at the PC boundary ($z = 0$). Inside the PC, the pulse propagates as a single refracted pulse to some depth $z < z_0$. In this case, all four waves exist at each PC point and the pendulum effect is observed (Fig. 5a), i.e., the field intensities for the transmitted (I_0) and diffracted (I_h) waves (20) are periodically distributed with a period of 2Λ along the z axis. At $z > z_0$, the pulse separates into two pulses each of which contains only one mode, the Borrmann or anti-Borrmann one, localized mainly in the region with a small or large refractive index, respectively (Fig. 5b). The separation between the pulses increases linearly with depth z. If the Bragg condition for the central wave packet frequency is fulfilled exactly, then the pulses propagate perpendicularly to the PC surface along the layers in a channel with a width of $2r_0/\cos\theta_B$. This is explained by the restoring action of diffraction reflection in the periodic structure on radiation. It is worth noting that the period of the intensity oscillations for the separated pulses along the x axis clearly seen in Fig. 4 differs from the true one (see Fig. 5b), because the spatial resolution of the graph presented in Fig. 4 is finite.

Each of the pulses that resulted from DIPS consists of the coincident (in space and time) transmitted and diffracted pulses coupled between themselves by dynamical diffraction. They separate only on the PC exit surface and, subsequently, each of them propagates in its own direction: the two transmitted pulses propagate along $\mathbf{k}_0$ and the two diffracted pulses propagate along $\mathbf{k}_h = \mathbf{k}_0 + \mathbf{h}$ (Fig. 4, $z > 4$ mm). The reflection from the lower boundary is disregarded; we assume that it is weak and does not change the characteristic shape of the field distribution at the exit from

the PC. The intensity of the incident pulse with amplitude A_{in} and the intensity of the specularly reflected (from the upper boundary) pulse with amplitude A_s are presented in the upper region of the free space (Fig. 4, $z < 0$), outside the structure. These distributions were obtained when the wave equation was solved in free space [22] with boundary conditions corresponding to the specified incident pulse field (18) on the upper PC surface ($z = 0$). The field distribution for the four pulses emerged in free space as a result of DIPS is presented in the lower part of the graph. The field distribution for the transmitted and diffracted field components (15) and (16) at $z = 4$ mm was used as the boundary condition.

3. SELECTIVE COMPRESSION AND FOCUSING OF THE BORRMANN AND ANTI-BORRMANN PULSES

The different dispersion laws for the Borrmann and anti-Borrmann pulse fields attributable to the lattice-induced dispersion in a linear PC upon Bragg diffraction in the Laue geometry (see Fig. 2) allow compression of one of the pulses and stretching of the other to be simultaneously executed in the case of a phase modulation of the incident signal. Let us show this using the propagation of spatially confined pulses with a quadratic phase modulation as an example.

The quadratic phase modulation in the direction of pulse propagation is specified by a linear frequency modulation, i.e., chirp, while the phase modulation in the transverse direction corresponds to wave packet focusing or defocusing. The complex envelope (1) of such a pulse on the PC surface can generally be represented as a generalization of Eq. (18):

$$A_{in}(x, t) = A_0 \exp\left[-\left(\frac{x\cos\theta}{r_0}\right)^2(1 - i\sigma) - \left(t - \frac{x\sin\theta}{c}\right)^2\frac{1 - i\beta}{\tau^2}\right],$$

where σ is the parameter that describes the phase change due to wave front bending (focusing or defocusing), the parameter β describes the linear change in pulse frequency, and A_0 is the amplitude of the incident field. The spectrum of such a wave packet calculated from Eq. (3) is

$$A_{in}(K, \Omega) = \tilde{A}_0 \exp\left[-\left(K - \frac{\Omega\sin\theta}{c}\right)^2\frac{1 + i\sigma}{\Delta K^2} - \frac{\Omega^2}{\Delta\Omega^2}(1 + i\beta)\right],$$

where

$$\Delta\Omega = \frac{2}{\tau}\sqrt{1 + \beta^2}, \quad \Delta K = \frac{2\cos\theta}{r_0}\sqrt{1 + \sigma^2}$$

are the characteristic widths of the spectrum for the frequency-modulated pulse and the x projection of the wave vector (due to the change in the angle of incidence of the pulse), $\tilde{A}_0$ is its amplitude. The width of the spatial frequency spectrum for modulated pulses is larger than that for nonmodulated ones, i.e., spectrally confined pulses with the same duration and transverse size. The parameters σ and β define the spectrum broadening upon modulation. Below, we will show that the noticeable changes in pulse duration and transverse size associated with the phase modulation of the incident pulse emerge when the pulse spectrum broadens significantly, i.e., at $|\sigma, \beta| \gg 1$.

For the convenience of calculating the group velocity projections, let us write the dispersion relation (12) as

$$q_{0z}^{(j)2} + q_{0x}^2 = q_0^{(j)2}(\omega, q_{0x}), \tag{21}$$

where

$$q_0^{(j)2}(\omega, q_{0x}) = \chi_0 k^2 + h\alpha_0 \mp \sqrt{h^2\alpha_0^2 + \chi_h\chi_{-h}k^4}$$

is the square of the magnitude of the wave vector for the forward wave in the PC and $\alpha_0 = q_{0x} - h/2$ defines the deviation of the x projection q_{0x} from the exact Bragg condition $q_{0x} = h/2$. The dispersion relation for the diffracted waves can be obtained by substituting $q_{0x} = q_{hx} + h$ and $q_{0z} = q_{hz}$ into (21). Equation (21) relates the variables q_{0x}, q_{0z}, and ω, which were previously independent in (5). The explicit dependence of q_0 on q_{0x} is explained by the lattice-induced dispersion in the PC. To find the group velocity projections, let us write the differential of Eq. (21) as

$$2q_{0z}^{(j)}dq_{0z}^{(j)} + 2q_{0x}dq_{0x} = \frac{\partial q_0^{(j)2}}{\partial\omega}d\omega + \frac{\partial q_0^{(j)2}}{\partial q_{0x}}dq_{0x}. \tag{22}$$

Provided that the variable $q_{0x} = \text{const}$, the z projection of the group velocity $v_z^{(j)} = (\partial\omega/\partial q_{0z}^{(j)})\big|_{q_{0x}}$ is then

$$v_z^{(j)} = \frac{cq_{0z}^{(j)}}{k(\chi_0 \mp \chi_h\chi_{-h}k^2/W)}, \tag{23}$$

where $q_{0z}^{(j)}$ can be determined from (21) and $W = \sqrt{h^2\alpha_0^2 + \chi_h\chi_{-h}k^4}$; as above, the plus and minus signs correspond to the Borrmann ($j = 1$) and anti-Borrmann ($j = 2$) modes, respectively. Assuming that the variable $q_{0z} = \text{const}$ in (22), we will obtain the following expression for the x projection of the group velocity $v_x^{(j)} = (\partial\omega/\partial q_{0x})\big|_{q_{0z}}$:

$$v_x^{(j)} = \frac{c\alpha_0(1 \pm h^2/2W)}{k(\chi_0 \mp \chi_h\chi_{-h}k^2/W)}. \tag{24}$$

The velocity $v_x^{(j)}$ is zero when the Bragg condition $\alpha_0 = 0$ is fulfilled exactly and changes its sign when the sign of the detuning α_0 changes. The group velocities for the diffracted waves (q_{hx}) can also be calculated from Eqs. (23) and (24), in which the substitutions

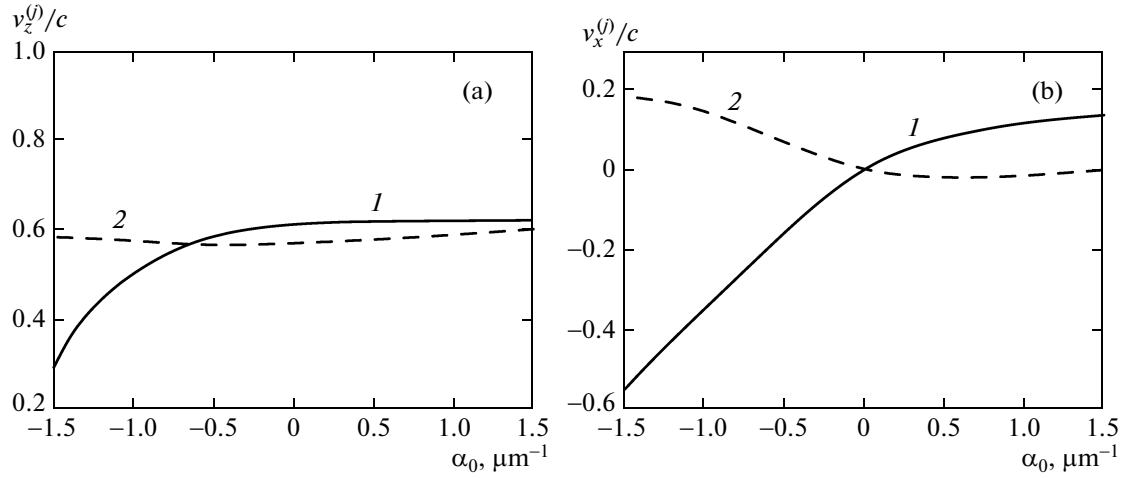

Fig. 6. Group velocity projections in a photonic crystal along the z (a) and x (b) axes normalized to the speed of light in a vacuum versus frequency Ω at a fixed angle of incidence $\theta = \theta_B$ for the Borrmann (curves *1*) and anti-Borrmann (curves *2*) modes; the Bragg detuning $\alpha_0 = q_{0x} - h/2 = (\Omega/c)\sin\theta_B$. The PC and radiation parameters are the same as those in Fig. 2.

$q_{0z} = q_{hz}$ and $\alpha_0 = \alpha_h$, where $\alpha_h = q_{hx} + h/2$ with $q_{hx} < 0$, should be made. Thus, the group velocities of the forward (q_{0x}, q_{0z}) and diffracted (q_{hx}, q_{hz}) waves for each mode, the Borrmann or anti-Borrmann one, coincide; therefore, we can talk about the group velocities of the Borrmann or anti-Borrmann pulse. As follows from (24), at $\alpha_0 < 0$, the anti-Borrmann pulse propagates in the forward direction ($v_x^{(2)} > 0$), while the Borrmann one propagates in the direction of diffraction-induced reflection ($v_x^{(1)} < 0$). In contrast, at $\alpha_0 > 0$, the Borrmann pulse propagates in the forward direction ($v_x^{(1)} > 0$), while the anti-Borrmann propagates in the opposite direction ($v_x^{(2)} < 0$). This can also be clearly seen from the directions of the group velocities in Fig. 2.

In Fig. 6, the group velocity projections (23) and (24) are plotted against the detuning α_0, i.e., actually on q_{0x}, provided that a transversally unconfined pulse is incident on the PC boundary at a given angle θ_B, where θ_B is the Bragg angle for the central frequency of the pulse spectrum. In this case, it follows from the boundary conditions that the waves with frequencies ω and wave vector projections $q_{0x} = k_x = (\omega/c)\sin\theta_B$ propagate in the PC. Therefore, when constructing the plots from Eqs. (23) and (24), we used the dependences $k = \omega/c$ and $q_{0x} = (\omega/c)\sin\theta_B$. It follows from the latter expression that a linear frequency modulation of the incident pulse leads to a linear modulation of the x projection q_{0x} of the wave vector in the PC.

We see from the plots in Fig. 6 that the lattice-induced dispersion $\partial v_{z,x}^{(1,2)}/\partial q_{0x}$ of the group velocities has the same sign for the Borrmann and anti-Borrmann modes for the z velocity projections $v_z^{(1,2)}$ (Fig. 6a) and opposite signs for the x projections $v_x^{(1,2)}$ (Fig. 6b) in a fairly wide range of α_0 values near the Bragg condition $\alpha_0 = 0$. The sign of the dispersion is retained when the sign of the velocity $v_x^{(1,2)}$ changes. This means that if a chirped pulse is incident on the PC, then, for example, the Borrmann pulse will compress along the x axis, while the anti-Borrmann one will spread due to different wave velocities $v_x^{(1,2)}$ at the leading and trailing pulse edges. The Borrmann and anti-Borrmann pulses will simultaneously either weakly compress or spread along the z axis, depending on the sign of the chirp, due to a weak dispersion of the group velocities of the same sign.

Figure 7 presents the spatial distribution of the sum of the magnitudes of the field amplitudes $|A_0| + |A_h|$ inside the PC calculated from Eqs. (16) for the diffraction of spatially confined pulses with chirps of opposite signs at opposite signs of the detuning α_0. For negative chirp ($\beta < 0$), the frequency of the leading edge of the incident pulse is lower than that of the trailing edge; q_{0x} also changes. Therefore, if the central pulse frequency is higher than the Bragg one, i.e., $\alpha_0 > 0$ (Fig. 7a), then, as we see from Fig. 6b, $v_x^{(1)} > 0$ for the Borrmann pulse and the velocity dispersion is positive. Therefore, the velocity $v_x^{(1)}$ of the trailing edge is higher than that of the leading edge and the Borrmann pulse will compress while propagating along the x axis. At the same time, the anti-Borrmann pulse, with a low velocity $v_x^{(2)} < 0$, will be essentially unchanged, because it will simultaneously weakly compress along the z axis (Fig. 6a) and weakly spread along the x axis. Precisely such dynamics is observed in Fig. 7a.

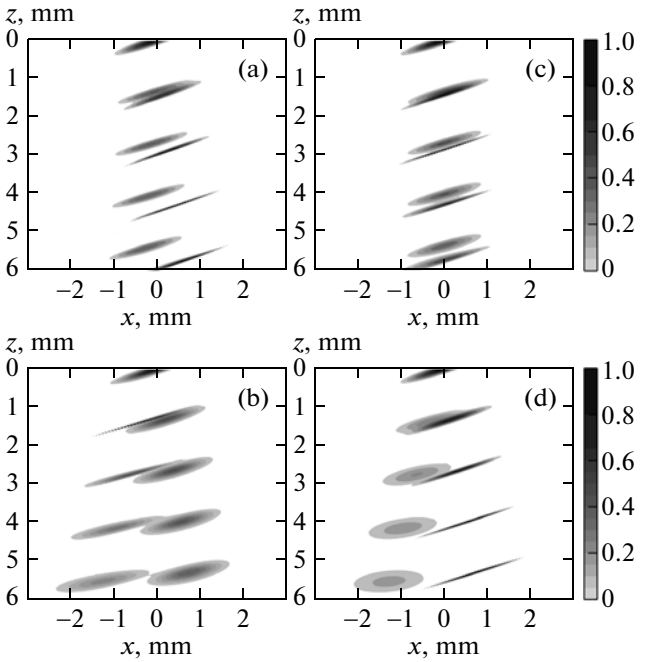

Fig. 7. Distribution of the sum of the magnitudes of the field amplitudes $|A_0| + |A_h|$ (rel. units) calculated from Eqs. (16) for the diffraction of chirped pulses. The parameters are $r_0 = 0.5$ mm, $\tau = 0.5$ ps, $d = 0.8$ μm, $n_1 = 1.7$, $\delta_0 = 0.2$, $\xi = 0.5$, and $\theta = 38.7°$. The Borrmann pulse compression: (a) $\beta = -15$, $\lambda_0 = 0.95$ μm, $\alpha_0 > 0$; (b) $\beta = -15$, $\lambda_0 = 1.1$ μm, $\alpha_0 < 0$; (c) $\beta = -15$, $\lambda_0 = 1$ μm, $\alpha_0 = 0$. The anti-Borrmann pulse compression: (d) $\beta = 15$, $\lambda_0 = 1.1$ μm, $\alpha_0 < 0$.

As the central pulse frequency decreases, the sign of α_0 changes ($\alpha_0 < 0$), the velocity of the Borrmann pulse becomes negative ($v_x^{(1)} < 0$), the dispersion increases (Fig. 6b), and it rapidly compresses (Fig. 7b). At the same time, the velocity of the anti-Borrmann pulse $v_x^{(2)} > 0$, the velocity dispersion is negative, and, therefore, it spreads (Fig. 7b). The exact fulfillment of the Bragg condition for the incident pulses, i.e., $\alpha_0 = 0$, causes Bormann pulse compression and anti-Borrmann pulse spreading at $\beta < 0$ (Fig. 7c). This is also in good agreement with the plots in Fig. 6b. The wave velocities at the central pulse frequency are zero in this case, $v_x^{(1, 2)} = 0$, but the velocities of the leading and trailing edges have opposite signs. For example, the velocities of the leading and trailing edge for the Borrmann pulse are, respectively, $v_x^{(1)} < 0$ (because $\alpha_0 < 0$) and $v_x^{(1)} > 0$ (because $\alpha_0 > 0$). Thus, at $\beta < 0$, the Borrmann pulse compresses at any detuning α_0. The change of sign of the chirp $\beta > 0$ at $\alpha_0 = 0$ leads to anti-Borrmann pulse compression and Borrmann pulse broadening. Finally, if $\alpha_0 < 0$ and $\beta > 0$, then, as follows from the plots in Fig. 6b, the anti-Borrmann pulse with $v_x^{(2)} > 0$ compresses, while the Borrmann one with $v_x^{(1)} < 0$ spreads (Fig. 7d). The anti-Borrmann pulse compresses at $\beta > 0$ in a wide range of α_0 values.

Thus, the selective compression of pulses, i.e., the compression of either fast pulses localized in PC layers with a smaller refractive index (Borrmann ones) or slow pulses propagating in layers with a larger refractive index (anti-Borrmann ones), can be executed by changing the sign of the chirp. The Borrmann and anti-Borrmann pulses can be interchanged in a specific direction of propagation by changing the sign of the detuning α_0 from the exact Bragg condition through a change in the central pulse frequency or the angle of incidence.

The pulse propagation directions in PCs under the DIPS effect are determined by the detuning of the center of the incident wave packet spectrum from the exact Bragg condition $\alpha_0 = 0$. In Figs. 7a, 7b, and 7d, the separated pulses propagate not parallel but at some angle to the PC layers, because the angle of incidence differs from the exact Bragg angle. In this case, pulses of fairly small transverse sizes emerge from the PC at different points of the PC exit surface, i.e., not only the temporal splitting or delay of the pulses but also their spatial shift inside the PC is realized. If the DIPS conditions break down in this case, then the pulses will leave the PC at different points but at the same instant of time.

The maximum pulse compression is achieved at a detuning from the Bragg condition when the entire incident radiation spectrum lies in the region of strong and approximately constant group velocity dispersion. Both a decrease in pulse duration and an increase in peak intensity (in our case, by a factor of 19) compared to an unchirped pulse are observed in this case (Fig. 8). Using pulses with considerably higher values of the parameter β allows a compression up to a factor of 30 to be achieved. An even larger compression can be realized only for a more complex (than the linear one) frequency modulation of the incident pulse corresponding to the compensation of the influence of higher-order dispersion.

When the pulse is incident at the exact Bragg angle, the pulse energy is evenly divided between the two modes. The amplitudes A_{gj} of each mode in Eqs. (16) and (17) for the amplitude transmission and reflection coefficients depend on the detuning α_0. As it increases, the intensity of one of the modes increases, while the intensity of the other mode decreases. This effect allows the detuning to be chosen in such a way that there is up to 80% of the entire field energy inside the PC in the compressing pulse. Such a case is presented in Fig. 8.

The compression (focusing) of pulses with a quadratic phase modulation ($\sigma \neq 0$) in the transverse direction with respect to the propagation direction is,

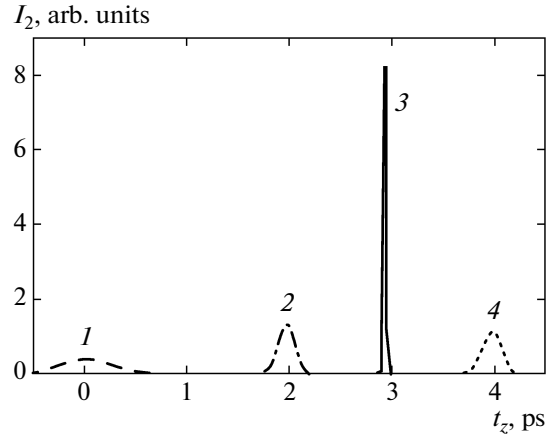

Fig. 8. Anti-Borrmann pulse intensities (20) versus time $t_z = t - z\gamma_0/c$ at various depths $z = 0$ (*1*), 4 (*2*), 5.8 (*3*), and 8 (*4*) mm inside a PC. The parameters are $\tau = 0.5$ ps, $\lambda_0 = 1.25$ μm, $\beta = -20$, $d = 1$ μm, $n_1 = 1.7$, and $\delta_0 = 0.2$.

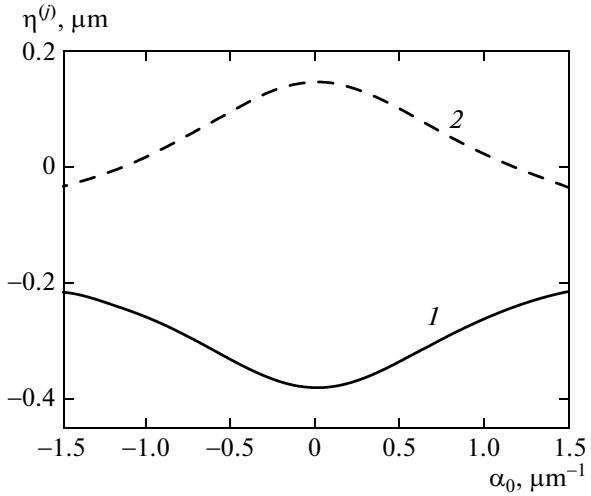

Fig. 9. Angular dependences of the transverse dispersion-induced pulse spreading parameters $\eta^{(j)}$ for the Borrmann (curve *1*) and anti-Borrmann (curve *2*) modes; $\alpha_0 = K$. The PC and radiation parameters are the same as those in Fig. 2.

on the whole, described just as in the case of a chirped pulse due to the spatiotemporal analogy [23]. In the approximations of a Gaussian wave packet profile, Fraunhofer diffraction, and a long pulse duration, we can obtain the following expression that describes the change in transverse pulse size:

$$r(z) = r_0\sqrt{\left(1 - \frac{2\sigma\eta z}{r_0^2}\right)^2 + \left(\frac{z}{L_\eta}\right)^2},$$

where $L_\eta = r_0^2/2|\eta|$ is the dispersion-induced broadening length and $\eta = \partial^2 q_{0z}/\partial q_{0x}^2$ is the parameter that characterizes the dispersion-induced wave packet spreading. The expression for η can be derived from the dispersion relation (21).

The quantities $\eta^{(1,2)}$ are plotted against the detuning in Fig. 9. It is important to note that $\eta^{(2)}$ is almost everywhere greater than zero for the anti-Borrmann mode and $\eta^{(1)} < 0$ for the Borrmann one. The magnitudes of $\eta^{(1,2)}$ have a maximum under the exact Bragg condition:

$$\eta^{(1,2)} = -\frac{1}{q_{0z}^{(1,2)}}\left(1 \pm \frac{h^2}{2k^2\sqrt{\chi_h\chi_{-h}}}\right).$$

The magnitudes of $\eta^{(1,2)}$ decrease as the detuning increases.

Two conditions should be met for the pulse compression in the transverse direction by focusing: the wave packet should have an initial modulation and the sign of σ should coincide with that of η. The violation of the first condition will lead to a monotonic increase in transverse pulse sizes upon diffraction, just as in the case of ordinary diffraction-induced spreading in a vacuum. The violation of the second condition will lead to a faster (relative to the propagation in a vacuum) broadening. Since $\eta^{(1,2)}$ have opposite signs, the sizes of not only the focused pulses but also the defocused ones, which can undergo only spatial spreading when propagating in a homogeneous medium, can decrease inside the PC.

Figure 10 presents the spatial distribution of the sum of the magnitudes of the field amplitudes (16) inside the PC for the diffraction of spatially modulated pulses. We see that when a defocused pulse is incident on the PC (Fig. 10a), the trailing anti-Borrmann pulse is focused (undergoes spatial compression) when propagating in the PC, while the leading Borrmann pulse is defocused, i.e., spreads. In contrast, in the case of a focused incident pulse, the Borrmann pulse compresses (Fig. 10b). Similar results are also obtained for the focusing of light beams upon diffraction in the Laue geometry in PCs, because the beams are a special case of spatially modulated wave packets whose longitudinal sizes are much greater than the transverse ones, i.e., $c\tau \gg r_0$.

It is important to emphasize that the DIPS and selective compression of separated pulses described here can take place only for the dynamical Bragg diffraction of radiation in the Laue geometry. These phenomena do not emerge if the Bragg diffraction scheme "for reflection" is used, because, in this case, there are only two [1] rather than four waves, as in the Laue scheme, propagating in the structure and no splitting of the incident pulse into the Borrmann and anti-Borrmann ones is possible. Note also that DIPS is essentially a coherent effect. As was shown in [24], taking into account the partial spatial and temporal coherences of radiation leads to deterioration of the observability of the dynamical diffraction phenomena, for example, to a smoothing of the pendulum effect.

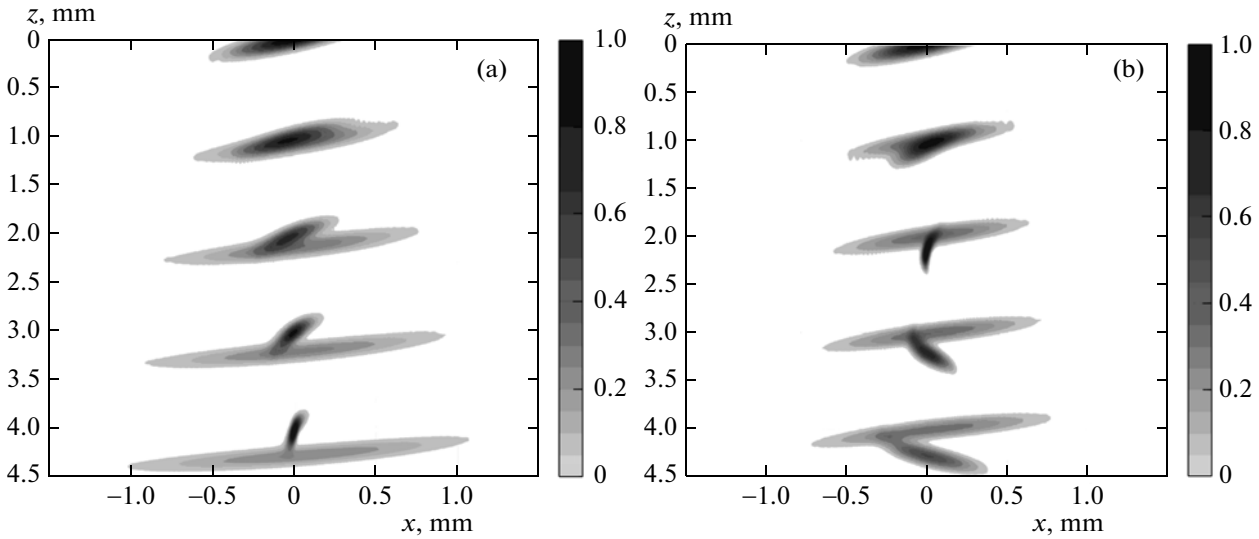

Fig. 10. Spatial distribution of the sum of the magnitudes of the field amplitudes $|A_0| + |A_h|$ (16) for the diffraction of spatially modulated pulses. The parameters are $r_0 = 0.25$ mm, $\tau = 0.5$ ps, $\lambda_0 = 1$ μm, $d = 0.8$ μm, $n_1 = 1.7$, $\delta_0 = 0.2$, $\xi = 0.5$, and $\theta = \theta_B = 38.7°$. (a) The incident pulse is defocused, $\sigma = 40$, the anti-Borrmann pulse is focused in the PC; (b) the incident pulse is focused, $\sigma = -40$, the Borrmann pulse is focused in the PC.

Therefore, in the case of diffraction of partially coherent radiation, one should expect a "blurring" of the perfect picture of the spatial field distribution corresponding to complete coherence of the diffracted waves (Fig. 5) and, as a consequence, a decrease in the efficiency (to the point of complete suppression) of diffraction-induced pulse splitting.

The spatial localization of the fields for the Borrmann and anti-Borrmann modes in the corresponding PC layers shown for spectrally confined pulses (see Fig. 5) is also observed in phase-modulated pulses undergoing compression inside the PC. The only noticed exception is the case where there is a significant detuning from the exact Bragg condition and the center of the incident radiation spectrum is shifted by a value of the order of the spectrum width. In this case, the amplitudes of the transmitted and diffracted waves in Eq. (15) are different; as a result, no standing waves are generated.

4. CONCLUSIONS

We theoretically described the dynamical Bragg diffraction of optical radiation in PCs—the diffraction-induced splitting of a spatially confined laser pulse incident on PCs in the case of diffraction in the Laue scheme. The selective compression and selective focusing of the separated pulses, the Borrmann and anti-Borrmann ones, have been predicted for the first time. These results are not only of fundamental interest but also of considerable applied one, because they allow new methods for controlling the dynamics and parameters of short laser pulses to be proposed. Indeed, the Borrmann and anti-Borrmann pulses actually propagate efficiently in different media due to their different spatial localizations in layers, respectively, with larger and smaller refractive indices of the structure. Therefore, by specifying different optical properties of the even and odd layers in the structure or, for example, by dynamically changing these properties with an external force, we can control the parameters (shape, polarization, amplitude, velocity, etc.) of the Borrmann and anti-Borrmann pulses independently. The selective compression and focusing of optical pulses will make it possible to considerably increase the yield of secondary, for example, nonlinear, processes in PCs by increasing the intensity of the Borrmann or anti-Borrmann pulse by more than an order of magnitude. In this case, nonlinear signals will be generated in different PC regions, predominantly in either even or odd layers of the structure, depending on the parameters of the input pulse—on the signs of the parameters of its frequency or spatial phase modulations and the detuning from the Bragg condition.

ACKNOWLEDGMENTS

This work was supported by the Russian Foundation for Basic Research (project nos. 09-02-00786 and 10-02-00768).

REFERENCES

1. Z. G. Pinsker, *X-Ray Crystal Optics* (Nauka, Moscow, 1982) [in Russian].
2. L. M. Brekhovskikh, *Waves in Layered Media* (Nauka, Moscow, 1973; Academic, New York, 1980).
3. G. Borrmann, Phys. Z. **42**, 157 (1941).

4. B. I. Mantsyzov, Opt. Commun. **189**, 275 (2001).
5. M. Calvo, P. Cheben, O. Martinez-Matos, F. del Monte, and J. A. Rodrigo, Phys. Rev. Lett. **97**, 084801 (2006).
6. V. A. Bushuev, B. I. Mantsyzov, and A. A. Skorynin, Phys. Rev. A: At., Mol., Opt. Phys. **79**, 053811 (2009).
7. S. Savo, E. Di Gennaro, C. Miletto, A. Andreone, P. Dardano, L. Moretti, and V. Mocella, Opt. Express **16**, 9097 (2008).
8. P. St. J. Russell, Phys. Rev. Lett. **56**, 596 (1986); P. St. J. Russell, J. Appl. Phys. **59**, 3344 (1986).
9. S. M. Arakelyan, L. P. Gevorkyan, and V. A. Makarov, Kvantovaya Elektron. (Moscow) **16**, 1846 (1989).
10. V. G. Baryshevsky and S. A. Maksimenko, Opt. Commun. **94**, 379 (1992).
11. O. Francescangeli, S. Melone, and R. De Leo, Phys. Rev. A: At., Mol., Opt. Phys. **40**, 4988 (1989).
12. B. Terhalle, A. Desyatnikov, D. Neshev, W. Krolikowski, C. Denz, and Y. S. Kivshar, Phys. Rev. Lett. **106**, 083902 (2011).
13. K. Busch, G. Von Freymann, S. Linden, S. F. Mingaleev, L. Tkeshelashvili, and M. Wegener, Phys. Rep. **444**, 101 (2007).
14. B. I. Mantsyzov, *Coherent and Nonlinear Optics of Photonic Crystals* (Fizmatlit, Moscow, 2009) [in Russian].
15. M. Scalora, M. J. Bloemer, A. S. Manka, J. P. Dowling, C. M. Bowden, R. Viswanathan, and J. W. Haus, Phys. Rev. A: At., Mol., Opt. Phys. **56**, 3166 (1997).
16. M. M. Fejer, G. A. Magel, D. H. Jundt, and R. L. Byer, IEEE J. Quantum Electron. **28**, 2631 (1992).
17. R. Fischer, S. M. Saltiel, D. N. Neshev, W. Krolikowski, and Yu. S. Kivshar, Appl. Phys. Lett. **89**, 191105 (2006).
18. I. V. Shutov, I. A. Ozheredov, A. V. Shumitski, and A. S. Chirkin, Opt. Spectrosc. **105** (1), 79 (2008).
19. F. Lederer, G. Stegeman, D. Christodoulides, G. Assanto, M. Segev, and Y. Silberberg, Phys. Rep. **463**, 1 (2008).
20. C. J. Benton and D. Skryabin, Opt. Express **17**, 5879 (2009).
21. L. A. Golovan, V. Yu. Timoshenko, and P. K. Kashkarov, Phys.—Usp. **50** (6), 595 (2007).
22. V. A. Bushuev, J. Synchrotron Radiat. **15**, 495 (2008).
23. S. A. Akhmanov, V. A. Vysloukh, and A. S. Chirkin, *Optics of Femtosecond Laser Pulses* (American Institute of Physics, New York, 1992; Nauka, Moscow, 1998).
24. S. A. Akhmanov, Yu. E. D'yakov, and A. S. Chirkin, *Introduction to the Statistical Radiophysics and Optics* (Nauka, Moscow, 1981), Sect. 6, Chap. 4 [in Russian].

Translated by V. Astakhov